Data-Driven Transmission Defense Planning Against Extreme Weather Events

Jiahao Yan, *Student Member, IEEE*, Bo Hu, *Member, IEEE*, Kaigui Xie, *Senior Member, IEEE*, Junjie Tang, *Member, IEEE*, and Heng-Ming Tai, *Senior Member, IEEE*

***Abstract*—Ensuring the resilience of power system is the prerequisite for maintaining its normal operation after the occurrence of natural disasters. This paper proposes a data-driven transmission defense planning (DTDP) model to address the power system resilience issue against extreme weather events. DTDP enables the determination of the optimal resilience enhancement portfolio, including line hardening and construction. The target events of DTDP are selected according to survivability based severity indices. The component survivability and post-disaster system failure state are treated as random variables in two separate levels, and the selected historical data are used to construct the confidence sets of their ambiguous probability distribution. Thus, the man-made uncertainty budget can be avoided and the expected economic loss under the worst-case distribution is minimized. Moreover, a sparsification method of system failure states is designed to boost computational efficiency. The effectiveness of DTDP and its solution method are verified on a six-bus test system and RTS-79 system. The results demonstrate that the DTDP can obtain a better defense plan compared to other optimization techniques.**

***Index Terms*—Transmission defense planning, power system resilience, distributionally robust optimization, extreme weather events, component survivability.**

NOMENCLATURE

Indices and Sets

Ω_F/s	Set/indices of system failure states that cause loadshed
Ω_{sa}/Ω_{su}	Set of components that survive/do not survive the extreme event in state s
Ω_{Fl}	Subset of Ω_F in whose failure states transmission line l fails
$\Omega^{TE}/e/N_e$	Set/indices/number of target extreme events
$\Omega^{RE}/n/N_p$	Set/indices/number of representative extreme events
$\mathbb{B}$	Feasible region of available defense plans
$\mathbb{D}$	Confidence set of probability distribution for the survivability vector
$\mathbb{W}$	Confidence set of probability distribution for the survivability vector
$\mathbb{O}$	Feasible region of system operation
Ω_S	Supporting space of the survivability vector for all transmission lines
Ω_z	Supporting space of failure status vector
Ω_{zK}	Subspace of Ω_z with K contingency level
$\Omega_l/l/N_l$	Set/indices/number of transmission lines
Ω_l^C	Set of candidate transmission lines
Ω_b/b	Set/indices of buses
Ω_g/m	Set/indices of generation units
$\Omega_l^+(b)/\Omega_l^-(b)$	Set of transmission lines flow into/out of bus b
$\Omega_g(b)$	Set of generation units connected to bus b
Ω_h/k	Set/indices of hardening plans.

Parameters

κ	Sensitivity factor of failure rate to wind speed
w_{thr}	Threshold wind speed for failure rate function
λ_{norm}	Component failure rate under normal condition
S_l^{norm}	Survivability of transmission line l under normal condition
f^{TE}	Annual average frequency of target events
ω_b^L	Unit cost of load shed at bus b
LD_b	Ratio of loadshed at bus b
P_b^L	Load demand at bus b
c_l^u	Investment cost for construction of transmission line l
c_{lk}^h	Investment cost for hardening of transmission line l with plan k
$\Gamma_{\max}$	Budget of defense planning
$P_{n,\min}^K/P_{n,\max}^K$	Upper/lower bound of K-level failure probability under representative event n
$K_{\max}$	Maximum contingency level
G_l/B_l	Conductance/susceptance of transmission line l
G_b^B/B_b^B	Shunt conductance/susceptance at bus b
$\underline{P_m^g}/P_m^g$	Upper/lower limits of real power output for generation unit m

Manuscript received June 19, 2019; revised September 16, 2019; accepted October 28, 2019. Date of publication October 31, 2019; date of current version April 21, 2020. This work was supported in part by the National Science Fund for Distinguished Young Scholars of China under Grant 51725701, and in part by the National Natural Science Foundation of China under Grant 51677011. Paper no. TSG-00858-2019. *(Corresponding author: Bo Hu.)*

J. Yan, B. Hu, K. Xie, and J. Tang are with the State Key Laboratory of Power Transmission Equipment and System Security, Chongqing University, Chongqing 400030, China (e-mail: yanjiahaojia@163.com; hboy8361@163.com; kaiguixie@vip.163.com; tangjunjie@cqu.edu.cn).

H.-M. Tai is with the Department of Electrical and Computer Engineering, University of Tulsa, Tulsa, OK 74104 USA (e-mail: tai@utulsa.edu).

Color versions of one or more of the figures in this article are available online at http://ieeexplore.ieee.org.

Digital Object Identifier 10.1109/TSG.2019.2950844

$\underline{V_b}/\overline{V_b}$	Upper/lower limits for voltage amplitude at bus b
$\underline{\theta_b}/\overline{\theta_b}$	Upper/lower limits for voltage angle at bus b
M	Large value constant.

Functions and Variables

$\lambda_t^w(\cdot)$	Component failure rate at time t during the extreme event
w_t	Wind speed at time t during the extreme event
$L(s)$	Loadshed of failure state s
S_l^e	Survivability of transmission line l under extreme event e
$S_{nl}(\cdot)$	Survivability of transmission line l under representative event n
u_l	Binary investment variables for transmission line construction
h_{lk}	Binary investment variables for transmission line hardening
$Q_n/\widehat{Q}_n$	Actual/Reference probability on the representative point n of survivability vector
r_n^+/r_n^-	Auxiliary variables for measuring the positive/negative deviation of Q_n from $\widehat{Q}_n$
$v_{nn'}^+/v_{nn'}^-$	Auxiliary variables for measuring the positive/negative transfer quantity from representative point n to n'
$d_{<n,n'>}$	Distance function between representative points n and n'
z_l	Failure Status of transmission line l
$P(\mathbf{z})$	Probability of failure status vector
P_m^g/Q_m^g	Real/reactive power output of generation unit m
P_l^f/Q_l^f	Real/reactive power flows on transmission line l
V_b/θ_b	Voltage amplitude/angle at bus b.

I. Introduction

THE INCREASINGLY frequent natural disasters are putting pressure on the current design of power systems. It has been reported [1] that the extreme weather events, although with low probability, account for a large proportion of power outages and loadshed worldwide. In December 2012, the hurricane Sandy swept the northeast region of the United States, causing a loss of more than 50 billion dollars [2]. The more recent super typhoon invading southeast coast of China tripped over 429 power lines, leaving more than 1.26 million households without power. These issues reveal the deficiency of most of the conventional planning methods currently adopted by power system planners and lead to their ill-preparedness in the face of extreme weather conditions.

Transmission defense planning (TDP) has been proposed to design the topology of transmission network so as to enhance its resilience under extreme events [3]. According to [4], resilience is defined as the ability to anticipate, adapt to and/or rapidly recover from disruptive events. With an emphasis on the adaptation, TDP can only achieve the best defense plan by following an accurate description of extreme event uncertainties [5].

Simulation based heuristics, scenario based stochastic optimization, and robust optimization are three common approaches to deal with TDP. Theoretically, the uncertainty of extreme weather events can be most accurately depicted by a simulation-based model. In [6], the non-sequential Monte-Carlo simulation and particle swarm algorithm are used to plan the optimal reliability parameters under normal condition. A sequential Monte-Carlo based simulation model was proposed to assess the effect of extreme weather and different enhancement measures on power system resilience [7]. In [8], a framework was designed to capture the uncertainties under severe weather conditions and dynamic system states. The wind field model was developed to quantify the grid resilience under a certain typhoon event [9]. The weather-induced interruptions were also predicted using the chronological data, considering multiple weather parameters [10]. The Boolean logic driven Markov process is utilized to simulate the dynamics of smart grid under variable weather conditions [11]. Nevertheless, the simulation under extreme events takes much more time than that under the normal condition. Thus, simulation based methods are not widely applied to determine the optimal combination of defense strategies.

In stochastic optimization, the expected system loss of all scenarios is set as the objective function. The scenario reduction technique has been used to cut down the computation time [12]. For example, six failure states corresponding to two earthquake events were considered to represent all possible scenarios [13]. The component states are sampled according to their failure probability to cope with the decision-dependent uncertainty [14], [15]. The roles of battery storage and photovoltaic generation in power system resilience were also studied [16]. The event-induced failures are characterized by the concept of capacity accessibility, and various scenarios are used to consider different patterns of PV generation. But the limited number of scenarios used in stochastic optimization often fails to represent the entire space of uncertain variables.

Several recent papers have considered the defender-attacker-defender (DAD) model to overcome the drawbacks of stochastic optimization [17]–[19]. The DAD model is initially designed to cope with the worst-case failure state under malicious attack. DAD requires fewer input data and is robust in preventing large scale power outages [20]. To capture the spatial-temporal dynamics of extreme weather, a multi-stage multi-zone uncertainty set was designed [21] and extended to the field of integrated electricity and natural gas system [22]. This approach was also adopted in similar problems with the renewable energy integration [23]. However, the current three-level DAD model has some shortcomings. One is it is not able to differentiate the failure probability of individual component. Another is the DAD model assumes that the hardened components are not influenced by the weather events. This assumption is not practical in engineering applications. Thus, approaches based on information theory have been proposed to adapt the uncertainty sets under the assumption that the failure of the component with lower failure probability takes up

larger uncertainty budget [24], [25]. The DAD models generally encounter the following deficiencies. 1) The model does not make full use of extreme events data. Instead, the results heavily rely on the uncertainty budgets, which may be prone to misjudgment. 2) DAD considers the cost-efficiency under the worst-case failure state only, not all the failure states. As a result, the situation of over-conservatism often occurs.

To overcome these challenges, this paper proposes a data-driven transmission defense planning (DTDP) model to enhance the system resilience against extreme weather events. DTDP is developed based on the distributionally robust optimization theory [26], [27]. Two primary defense measures, the line hardening and the line construction, are coordinated to yield the optimal scheme. The DTDP model learns the spatial distribution of weather intensity from historical meteorological data, which are transformed into component survivability by fragility models to represent the marginal probability of post-event system failure states. Thus, the proposed DTDP model does not need weather-related failure records to infer credible failure probability distributions of transmission lines.

Contributions of the paper include the following:

- Propose severity indices of extreme weather events to select the input data for the DTDP so that a tradeoff between the resilience and cost can be achieved.
- Establish a four-level DTDP model. The model uses historical data of extreme events to treat the uncertainties of disaster intensity and system failure states in two separate levels, while minimizing the expected economic loss under the worst-case probability distribution. It is less conservative than the traditional DAD model and is able to differentiate the failure probabilities of different transmission lines under various extreme events.
- Devise a sparsification method to reduce the number of failure states used in the DTDP model so that the computational efficiency is improved significantly.

The rest of this work is organized as follows: Section II presents the concept of component survivability and the selection of target extreme events. Section III describes the framework of DTDP model. Section IV introduces the solution method of DTDP. Numerical results obtained from a modified 6-bus and IEEE RTS-79 systems are presented to demonstrate the effectiveness of the proposed method in Section V. Section VI draws the conclusion.

II. Selection of Target Extreme Events

The data selection of extreme events is important for DTDP. For example, events with severe consequences but low occurrence rate could be ignored in the initial stage due to substantial investment required to deal with them. However, these events could be included given that the utility owners seeks to improve the system resilience further. In this section, the concept of component survivability is presented firstly, which is then used to select the target events for DTDP.

A. Component Survivability

Component failure in an extreme weather event has the following characteristics:

- The duration of extreme weather event is very short compared to that of normal weather condition.
- As it is difficult to commit restoration effort under extreme weather, the status of a component typically remains unchanged once it fails until the end of the event.

Therefore, from the perspective of a long-term planning problem, it makes sense to judge the severity of an extreme event by the post-event outage scenario at its end time. Realization of these outage scenarios can be decided by the component survivability. The component survivability is defined as the probability of a component maintaining its normal operation after going through an extreme weather event.

In this paper, windstorm is regarded as the primary event type and only its influence on overhead transmission lines is considered. Hence, the component survivability is directly derived from fragility model in [28], in which the failure rate of any component at time t can be expressed as:

$$\lambda_t^w(w_t) = \left[1 + \kappa\left(\frac{w_t^2}{{w_{\text{thr}}}^2} - 1\right)\right] \cdot \lambda_{\text{norm}} \tag{1}$$

where w_{thr} represents the wind speed threshold starting to affect the failure rate. κ represents the sensitivity factor of failure rate to wind speed at time t, w_t. Larger κ implied the component is more vulnerable to the strong wind. λ_{norm} represents the failure rate under normal condition. The failure rate starts to rise once the wind speed rise above w_{thr}.

Then, the component survivability can be calculated using the survival function [29]:

$$S(t_e|t_0) = P(z(t_e) = 0|z(t_0) = 0) = \exp\left\{-\int_{t_0}^{t_e} \lambda_t^w(w_t)\mathrm{d}t\right\} \tag{2}$$

where t_0 and t_e denotes the start and end of the studied extreme event. $z(t)$ represents the component damage status at time t (1 denotes the damage status and 0 otherwise).

Next, a transmission line composed of its conductor and towers is considered. The overall survivability of a transmission line can be expressed as

$$S_l^e = 1 - \prod_{i=1}^{N_{lp}} \left(-S_{li}^e\right) \prod_{j=1}^{N_{lc}} \left(1 - S_{lj}^e\right) \tag{3}$$

where S_l^e, S_{li}^e and S_{lj}^e represent the survivability of transmission line l, the i^{th} tower of l and the j^{th} segment of its conductor in the extreme event e, respectively. N_{lp} denotes the number of towers in transmission line l and N_{lc} the number of conductor segments.

B. Target Events Selection Based on Severity Index

1) Exact Indices: The power system may have many potential failure states after extreme events. The severity of these events can be identified by the exact indices using component survivability.

1) Post-event Loss of Load Probability (LOLP-E)

$$LOLP - E = \sum_{s \in \Omega_F} \left(\prod_{l \in \Omega_{sa}} S_l^e \prod_{l \in \Omega_{su}} \left(1 - S_l^e\right) \right) \tag{4}$$

2) Post-event Expected Power Not Supplied (EPNS-E)

$$EPNS-E=\sum_{s\in\Omega_F}\left[\left(\prod_{l\in\Omega_{sa}}S_l^e\prod_{l\in\Omega_{su}}\left(1-S_l^e\right)\right)\cdot L(s)\right] \quad (5)$$

where Ω_F is the set of scenarios that lead to the loadshed of system. Ω_{sa} represents the set of components that survive the extreme event in state s, and Ω_{su} those do not survive. $L(s)$ denotes the loadshed of state s. These two indices are exact as they account for all the potential failure states. Moreover, they can be used to evaluate the system robustness after defense planning.

2) Approximate Index: The calculation of above indices can be time-consuming. Since a large number of candidate events need to be checked before running the DTDP model, an approximate index, Weighted Component Survivability Deterioration Ratio (WCSDR), is developed for fast screening.

$$WCSDR=\frac{\sum_{l\in\Omega_l}FPF_l\left(S_l^{\text{norm}}-S_l^e\right)/S_l^{\text{norm}}}{N_l} \quad (6)$$

where

$$FPF_l=\frac{\sum_{s\in\Omega_{Fl}}L(s)}{\sum_{s\in\Omega_F}L(s)} \quad (7)$$

S_l^{norm} is the survivability of transmission line under the normal weather condition. Ω_{Fl} is a subset of Ω_F that transmission line l does not survive the event. FPF_l represents the failure participation factor that signify the importance of each component. It only has to be calculated once for all extreme events.

The events with the severity index in the target range will be included in a set Ω^{TE} and is served as the input data to the DTDP model.

III. Proposed DTDP Model

A. Model Overview

The DTDP intends to deal with the uncertainty of disaster intensity and system failure states simultaneously. Considering the correlations between these two kinds of uncertainties, the overall formulation of DTDP can be expressed in (8), as shown at the bottom of the next page, and depicted as a four-level model shown in Fig. 1.

The objective of DTDP is to minimize the expected loss of load as a consequence of potential extreme events. The highest level (Level I) decides the optimal defense plan and is named the planning decision problem (PDP). Level II accepts historical information on all extreme events and deals with the probability distribution of disaster intensity. It is called the long-term performance problem (LPP). Level III uses the component survivability modified by hardening decisions to handle the probability of failure states. It is called the short-term performance problem (SPP). Level IV is the lowest level and is also called the system response problem (SRP). It gives the optimal response to a certain failure state considering newly constructed lines.

In (8), $\boldsymbol{u}$ and $\boldsymbol{h}$ are the decision variables of line installation and hardening, respectively. $\boldsymbol{x}$ is the system dispatch variables

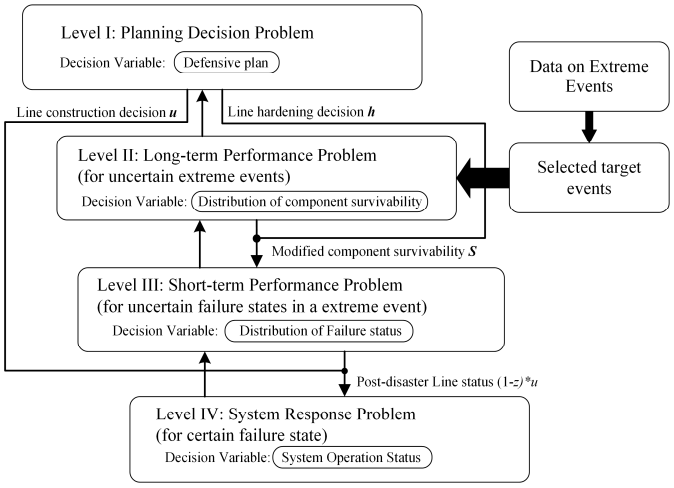

Fig. 1. The proposed framework of data-driven transmission defense planning.

under failure states. ω_b^L, LD_b and P_b^L represents the unit cost of loadshed, the ratio of loadshed and the load demand at bus b, respectively. $\mathbb{B}$ is the set of available line installation and hardening strategies. $\mathbb{O}$ is the feasible region of system operation conditions. $\boldsymbol{S}$ represents the vector of survivability for all transmission lines and Ω_S denotes the support of its probability density $\boldsymbol{Q}(\boldsymbol{S})$. f^{TE} is the annual average frequency of the target events and $\boldsymbol{z}$ represents the post-disaster status of transmission lines with its probability $\boldsymbol{P}(\boldsymbol{z})$ defined on Ω_z.

The linchpin of the DTDP model lies in the characterization of uncertainties of extreme events by the two max(·) operations in the middle of (8). These two operations are discussed below.

• The first max(·): Intuitively, the transmission lines located in the coastal region are more vulnerable to extreme weather such as typhoon. To quantify this knowledge, the vector of component survivability $\boldsymbol{S}$ in the first max(·) is treated as a multivariate uncertain variable (unlike S_l^e in Section II, which are determined for each specific event and treated as samples of $\boldsymbol{S}$ here) since they reflect the pattern of disaster intensity under different events. $\boldsymbol{S}$ is assumed to follow an ambiguous distribution because it only can be learned from a limited number of samples in Ω^{TE}. In other word, its probability density function (PDF), $\boldsymbol{Q}(\boldsymbol{S})$, is allowed to fluctuate within an confidence set $\mathbb{D}$ and max(·) is used to hedge against the worst realization of $\boldsymbol{Q}(\boldsymbol{S})$. Detailed formulation of $\mathbb{D}$ is discussed in Section III-B.

• The second max(·): To represent the uncertainty of post-disaster system state, $\boldsymbol{z}$ is regarded as an uncertain variable. The confidence set of its distribution, $\mathbb{W}$, is directly determined by the line survivability $\boldsymbol{S}$ delivered from the upper level, which will be detailed later in Section III-C. The expression in the second max(·) can be viewed as a system performance indicator once $\boldsymbol{S}$ is fixed. It has advantages over both EPNS-E in Section II and the maximum N-k contingency loadshed used in the three-level DAD model. Compared to EPNS-E, it emphasizes the scenarios with larger loadshed by the max(·) that the decision makers expects to dodge. The max(·) operation only requires the marginal probability of failure states,

thus remains tractable for solution when a lot of failure states are considered. Compared to the worst-case loadshed, it is still an expected value as it integrates the system performance under all failure states in Ω_z, rather than just the worst state.

Each problem in model (8) can be expressed as the following equations:

$$PDP = \min_{(\boldsymbol{u},\boldsymbol{h})\in\mathbb{B}} LPP(\boldsymbol{u},\boldsymbol{h}) \tag{9}$$

$$LPP(\boldsymbol{u},\boldsymbol{h}) = \max_{\boldsymbol{Q}(\boldsymbol{S})\in\mathbb{D}} f^{TE}\int_{\Omega_s} SPP(\boldsymbol{u},\boldsymbol{h},\boldsymbol{S})\mathrm{d}Q(\boldsymbol{S}) \tag{10}$$

$$SPP(\boldsymbol{u},\boldsymbol{h},\boldsymbol{S}) = \max_{\boldsymbol{P}(z)\in\mathbb{W}(\boldsymbol{S},\boldsymbol{h})}\int_{\Omega_z} SRP(\boldsymbol{u},z)\mathrm{d}\boldsymbol{P}(z) \tag{11}$$

$$SRP(\boldsymbol{u},z) = \min_{\boldsymbol{x}\in\mathbb{O}(\boldsymbol{u},z)}\sum_{\forall b}\omega_b^L LD_b P_b^L \tag{12}$$

Details of each problem are given in the subsequent sections.

B. Planning Decision Problem

The planning decision problem is designed to obtain an optimal planning decision while minimizing the objective of lower level problems. The available set for these planning decisions can be expressed as:

$$\mathbb{B} = \left\{ \boldsymbol{u},\boldsymbol{h} \left| \begin{array}{ll} \sum_{k\in\Omega_h} h_{lk} = 1 & (13.a)\\ u_l = 1 \forall l \in \Omega_l^E & (13.b)\\ \sum_{l\in\Omega_l^C} c_l^u u_l + \sum_{l\in\Omega_l}\sum_{k\in\Omega_h} c_{lk}^h h_{lk} = \Gamma_{\max}. & (13.c) \end{array} \right. \right\} \tag{13}$$

In (13), h_{lk} are the line hardening decision variables and u_l the line construction decision variables. h_{lk} is set to 1 once the k^{th} hardening plan is chosen for transmission line *l*. u_l is set to 1 if line l is constructed. c_l^u and c_{lk}^h are the cost of the line construction and hardening respectively. Constraints (13.a) state that only one hardening plan can be chosen for each transmission line. Constraints (13.b) force the u_l of the existing transmission line to be 1. Constraints (13.c) set an upper bound on the total defense budget allocated to line construction and hardening.

C. Long-Term Performance Problem

LPP aims to obtain the expected economic loss under the uncertain distribution of disaster intensity represented by $\boldsymbol{S}$.

It is not possible to ascertain the exact probability density on each point of Ω_s. Thus, N_p discrete representative points (RP) are used to represent the continuous space of component survivability. The values of RPs and their reference distribution $\widehat{\boldsymbol{Q}}$ can be calculated from the set of target events, Ω^{TE}. The procedure is described by Algorithm 1. Denote the survivability vector and actual probability of the n^{th} RP as Q_n and $\boldsymbol{S}_n$,

Algorithm 1 The Calculation of Representative Points and Reference Distribution in LPP

Step 1: Classify the target events according to the K-means algorithm, and set the centroid of each cluster at each RP, S_n.
Step 2: Calculate the Euclidian distance between target event and representative point. For example, the distance between the i^{th} element in Ω^{TE} and the n^{th} RP is

$$d_{<i,n>} = \|S_i - S_n\|_2. \tag{15}$$

Step 3: Allocate each element in Ω^{TE} to the corresponding representative point with minimum distance. Calculate the number of elements allocated to each RP, $\boldsymbol{F}$. The reference distribution for RPs can be obtained

$$\widehat{\boldsymbol{Q}} = \left[\frac{F_1}{F_T}, \frac{F_2}{F_T}, \ldots, \frac{F_n}{F_T}\right]. \tag{16}$$

the LPP of (10) is rewritten as:

$$LPP(\boldsymbol{u},\boldsymbol{h}) = \max_{\boldsymbol{Q}(\boldsymbol{S})\in\mathbb{D}} f^{TE}\sum_{n=1}^{N_p} Q_n \cdot SPP(\boldsymbol{u},\boldsymbol{h},\boldsymbol{S}_n). \tag{14}$$

As mentioned in Section III-A, the reference distribution $\widehat{\boldsymbol{Q}}$ could deviate from the actual distribution $\boldsymbol{Q}$ as it is obtained through finite target events. Since $\boldsymbol{Q}$ is not exactly known, it is allowed to take any value in a $\widehat{\boldsymbol{Q}}$-centered confidence set (17).

$$\mathbb{D} = \left\{ \boldsymbol{Q}\in[0,1]^{\mathrm{n}} \left| \begin{array}{ll} \sum_{n=1}^{N_p} Q_n = 1 & (17.a)\\ L_1 = \sum_{n=1}^{N_p}\left(r_n^+ + r_n^-\right) = \alpha_1 & (17.b)\\ L_\infty = r_n^+ + r_n^- = \alpha_\infty & (17.c)\\ \widehat{Q}_n + r_n^+ - r_n^- = Q_n,\ \forall nv & (17.d)\\ L_w = \sum_{\forall(n,n')} d_{<n,n'>}\left(v_{nn'}^+ + v_{nn'}^-\right) \le \alpha_W & (17.e)\\ \widehat{Q}_n + \sum_{n'}\left(v_{nn'}^+ - v_{nn'}^-\right) = Q_n, \forall n & (17.f)\\ r_n^+, r_n^-, v_{nn'}^+, v_{nn'}^- = 0, \forall n, n' & (17.g) \end{array} \right. \right\} \tag{17}$$

Constraint (17.a) states that the sum of probability must be equal to 1. Constraints (17.b)-(17.d) use non-negative variables r_n^+, r_n^- to measure the 1-norm distance, L_1, and the ∞-norm distance, L_∞. The Wasserstein distance L_w is constrained in (17.e). The upper bounds of L_1, L_∞ and L_w under confidence level β are given, respectively, by (18), (19), and (20) [30]:

$$\alpha_1 = \frac{N_p}{2N_e}\ln\frac{2N_p}{1-\beta} \tag{18}$$

$$\alpha_\infty = \frac{1}{2N_e}\ln\frac{2N_p}{1-\beta} \tag{19}$$

$$\alpha_w = l_S\sqrt{\frac{2}{N_e}\cdot\log\left(\frac{1}{1-\beta}\right)} \tag{20}$$

$$\min_{(\boldsymbol{u},\boldsymbol{h})\in\mathbb{B}}\max_{\boldsymbol{Q}(\boldsymbol{S})\in\mathbb{D}}\left\{ f^{TE}\int_{\Omega_S}\left[\max_{\boldsymbol{P}(z)\in\mathbb{W}(\boldsymbol{S},\boldsymbol{h})}\int_{\Omega_z}\min_{\boldsymbol{x}\in\mathbb{O}(\boldsymbol{u},z)}\sum_{\forall b}\omega_b^L LD_b P_b^L \mathrm{d}P(z)\right]\mathrm{d}Q(\boldsymbol{S})\right\} \tag{8}$$

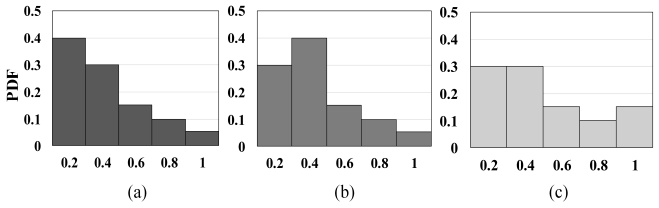

Fig. 2. The distribution distance between the reference distribution and the actual distribution. (a) Reference distribution. (b) Actual distribution 1, $L_1 = 0.2$, $L_\infty = 0.1$, $L_w = 0.02$. (c) Actual distribution 2, $L_1 = 0.2$, $L_\infty = 0.1$, $L_w = 0.08$.

Although L_1 and L_∞ are sufficient to ensure that $\boldsymbol{Q}$ is identical to $\widehat{\boldsymbol{Q}}$ when infinitely many target events are fed into LPP [31], the Wasserstein distance L_w modelled in (17.e-17.f) facilitates its convergence. The metric L_w assumes that $\widehat{\boldsymbol{Q}}$ could be transformed into $\boldsymbol{Q}$ by "transferring" the probability of the RP, n, to that of another RP, n', with the per unit cost equal to the distance between them. The distance $d_{<n,n'>}$ can be gauged by $v^+_{nn'}$ and $v^-_{nn'}$. The advantage of L_w is illustrated in Fig. 2. Suppose that Fig. 2(a) depicts the shape of reference distribution, $\widehat{\boldsymbol{Q}}$, while 2(b) and 2(c) depict two actual distributions defined on $\mathbb{D}$. The horizontal axis stands for the supporting space and the vertical axis the probability density of the distribution. Despite that distribution (b) resemble distribution (a) more than (c), their L_1 and L_∞ distance to (a) remain the same. Their difference can only be set apart by L_w. This implies that L_w enforces a stricter bound on the size of $\mathbb{D}$ than L_1 and L_∞, preventing the overestimation issue for LPP.

D. Short-Term Performance Problem

Once an RP of component survivability is delivered from the upper-level LPP, SPP managed to minimize the expected system loss under the worst-case probability distribution of system failure states. The confidence set $\mathbb{W}$ can be expressed as (21):

$$\mathbb{W}(\boldsymbol{S}_{\mathrm{n}}, \boldsymbol{h}) = \left\{ \boldsymbol{f}(\boldsymbol{z}) \in \mathrm{R}^{+}(\Omega_z) \;\middle|\; \begin{array}{ll} \int_{\Omega_z} P(\boldsymbol{z})\mathrm{d}\boldsymbol{z} = 1 & (21.\mathrm{a}) \\ \int_{\Omega_z} z_l \mathrm{d}P(\boldsymbol{z}) = 1 - S_{nl}(h_{lk}), \forall l & (21.\mathrm{b}) \\ P^K_{n,\min} \le \int_{\Omega_{zK}} P(\boldsymbol{z})\mathrm{d}\boldsymbol{z} \le P^K_{n,\max}, \forall K & (21.\mathrm{c}) \\ \Omega_z = \left\{ \boldsymbol{z} \in \{0,1\}^{N_l} \;\middle|\; \begin{array}{c} |\boldsymbol{z}| = K_{\max}, \\ \forall l \in \Omega_l \end{array} \right\} & (21.\mathrm{d}) \end{array} \right\} \tag{21}$$

Here, post-disaster line status vector $\boldsymbol{z}$ is assumed to be a N_l-dimension binary vector, with value 1 assigned to the corresponding outaged line. Ω_{zK} represents the subspace of failure states with K contingency level (those states that contain K line failures). Constraint (21.a) describes the basic property of probability distribution similar to (17.a). Constraints (21.b) ensures that the probability distribution of failure states share the same marginal probability as its original distribution used in the calculation of EPNS − E, regarding each transmission line. Constraint (21.c) restricts the probability of failure states with K contingency level. Constraint (21.d) states that up to $K_{\max}$ line outages are considered in the outage scenario. The outage scenario with more than $K_{\max}$ outages is considered to have a trivial probability and is neglected.

$S_{nl}(h_k)$ in (21.b) represents the component survivability of the n^{th} RP in LPP, corrected by the k^{th} hardening strategy in PDP. Constraints (21.b) are essential to ensure that the improvement of component survivability will lead to a shrinking feasible region defined by $\mathbb{W}$. This will immediately result in the decrease of (11) because (11) is maximized over $\mathbb{W}$. Moreover, note that only z_l participated in the left side (21.b). Therefore, the change of S_{nl} only impacts the system states that involve the failure of line l. Therefore, the hardening of the line whose failure contributes more to the loadshed will be prioritized.

The probability of high-level failure states with severe consequence could still be exaggerated if only (21.b) is enforced. Thus, (21.c) is introduced. The probability of K-level failure states is bounded by an interval $[P^K_{n,\min}, P^K_{n,\max}]$, rather than a fixed value, because its exact value could be revealed once the hardening strategy is determined in PDP. The probability of K-level failure states corresponding to the optimal defense plan is allowed to lie on any point within this interval. This interval can be estimated following Algorithm 2.

Algorithm 2 Probability Interval Estimation of K-Level Failure States

Step 1: Calculate the survivability under each hardening strategy for all transmission lines. The minimum and maximum value for each line are denoted as $S_{nl,\min}$ and $S_{nl,\max}$.

Step 2: Set the iteration index $i = 1$ for each line l. Initialize its current survivability $S^1_{nl} = S_{nl,\min}$. Calculate the K-level failure state probability, $P^K_{n,h1}$, using the stratified sampling method [32]. Set the update step of survivability to $\Delta S_{nl} = \frac{S_{nl,\max} - S_{nl,\min}}{N_c}$, where$N_c$ is the total iteration number.

Step 3: $i = i+1$. If $i > N_c$, then STOP. Determine the upper and lower bounds for the probability of K-level failure states by

$$\begin{cases} P^K_{n,\min} = \min\left(P^K_{n,h1}, P^K_{n,h2}, \ldots, P^K_{n,hN_c}\right) \\ P^K_{n,\max} = \max\left(P^K_{n,h1}, P^K_{n,h2}, \ldots, P^K_{n,hN_c}\right) \end{cases}, \ \forall K = K_{\max} \tag{22}$$

Otherwise, GOTO Step 4.

Step 4: Update the survivability of each line by $S^v_{nl} = S^{v-1}_{nl} + \Delta S_{nl}$. Calculate the corresponding probability of K-level Failure states, $P^K_{n,hv}$. GOTO **Step 3**.

E. System Response Problem

SRP can be expressed as in (23). It provides the optimal system response towards a certain failure state $\boldsymbol{z}$. Fuel cost of the generating units is omitted because the loadshed cost is the primary concern in a defense planning model. The transmission line repair is not considered in the model because the repair time and the available resources (such as repair crews, spare components) are difficult to estimate at the planning stage. Nevertheless, SRP does not pose problems in integrating the repair dispatch model such as [33] and [34], which

will be addressed in the future research.

$$\mathbb{O}(u,z) = \left\{ \boldsymbol{x} \;\middle|\; \begin{array}{rl} \sum_{m\in\Omega_g(b)} P_m^g + \sum_{l\in\Omega_l^+(b)} P_l^f = G_b^B(2V_b-1) & \\ \quad + (1-LD_b)P_b^L + \sum_{l\in\Omega_l^-(i)} P_l^f \forall b \in \Omega_b & (23.a) \\ \sum_{m\in\Omega_g(b)} Q_m^g + \sum_{l\in\Omega_l^+(b)} Q_l^f = -B_b^B(2V_b-1) & \\ \quad + (1-LD_b)Q_b^L + \sum_{l\in\Omega_l^-(b)} Q_l^f \forall \mathrm{b} \in \Omega_b & (23.b) \\ -(z_l+1-u_l)M \le P_l^f - \left[G_l\left(V_{s(l),t} - V_{e(l),t}\right)\right. & \\ \left. - B_l\left(\theta_{s(l),t} - \theta_{e(l),t}\right)\right] \le (z_l+1-u_l)M, \forall l \in \Omega_l & (23.c) \\ -(z_l+1-u_l)M \le Q_{l,t}^f + \left[B_l\left(V_{s(l),t} - V_{e(l),t}\right)\right. & \\ \left. + G_l\left(\theta_{s(l),t} - \theta_{e(l),t}\right)\right] \le (z_l+1-u_l)M, \forall l \in \Omega_l & (23.d) \\ u_l\underline{P_l^f} \le P_{l,t}^f \le u_l\overline{P_l^f}, \forall l \in \Omega_l & (23.e) \\ (1-z_l)\underline{P_l^f} \le P_{l,t}^f \le (1-z_l)\overline{P_l^f}, \forall l \in \Omega_l & (23.f) \\ \underline{P_m^g} \le P_m^g = \overline{P_m^g}, \forall m \in \Omega_g & (23.g) \\ \underline{V_b} \le V_b \le \overline{V_b}, \forall b \in \Omega_b & (23.h) \\ \underline{\theta_b} \le \theta_b \le \overline{\theta_b}, \forall b \in \Omega_b & (23.i) \\ 0 \le LD_b \le 1, \forall b \in \Omega_b & (23.j) \end{array} \right\} \tag{23}$$

A linear programming approximation of AC power flow (LPAC) in [35] is adopted in (23). Constraints (23.a) and (23.b) establish the nodal active/reactive power balance equation. Constraints (23.c)-(23.f) model the transmission line flow and then restrict them to their capacity. For a candidate line, if it is not built ($u_l = 0$) or fails due to extreme weather ($z_l = 1$), its line flow is forced to be 0. The allowable range for generating unit output, voltage amplitude, voltage angle and loadshed are specified in (23.g)-(23.j).

IV. Solution Method and Failure State Sparsification

In this section, the solution method of DTDP model is discussed. A simplified model using the sparsification method is developed to reduce the computational complexity.

A. Solution Method

The max(·) in the two middle levels disabled the direct solution of the DTDP model. Since numerous states exist in Ω_z, SPP could be deemed approximately as a semi-infinite programming problem with infinite variables.

The structures of the two upper levels are discussed first. The objective of SPP for each RP of LPP are denoted as a vector $\boldsymbol{SPP} = [SPP(\boldsymbol{u},\boldsymbol{h},S_1),\ldots,SPP(\boldsymbol{u},\boldsymbol{h},S_n)]^{\mathrm{T}}$, and (8) can be written in a compact mathematical form:

$$\min_{\boldsymbol{u},\boldsymbol{h}} \ \max_{\boldsymbol{Q}} \boldsymbol{SPP}^{\mathrm{T}}\boldsymbol{Q} \tag{24.a}$$

$$\text{s.t.} \ \ \mathbf{C}\boldsymbol{u} + \mathbf{D}\boldsymbol{h} \ge \boldsymbol{d} \tag{24.b}$$

$$[\mathbf{I}_{N_p}\mathbf{I}_{N_p}]^{\mathrm{T}}\left(\boldsymbol{Q} - \widehat{\boldsymbol{Q}}\right) = \mathbf{F}\boldsymbol{r} + \mathbf{G}\boldsymbol{v} : [\boldsymbol{\varepsilon}] \tag{24.c}$$

$$\mathbf{H}\boldsymbol{r} + \mathbf{I}\boldsymbol{v} \le \boldsymbol{\alpha} : [\boldsymbol{\mu}] \tag{24.d}$$

where $\mathbf{C}$ to $\mathbf{I}$ denotes the parameter matrix to the corresponding variables. $\boldsymbol{d}$ and $\boldsymbol{\alpha}$ represents the right hand side constants. $\boldsymbol{r}$ and $\boldsymbol{v}$ represents the vector of r_n^+, r_n^- in (17.b) and $v_{nn'}^+, v_{nn'}^-$ in (17.e). $\mathbf{I}_{N_p}$ denotes a N_p-dimension identity matrix. Constraint (24.b) represents (13). Constraint (24.c) represents (17.a), (17.d) and (17.f). Constraint (24.d) represents (17.b), (17.c) and (17.e). ε and μ are the dual variables of the corresponding constraints.

(25) can be obtained by dualizing the maximization problem in the lower level in (24) :

$$\min_{\boldsymbol{u},\boldsymbol{h},\boldsymbol{\varepsilon},\boldsymbol{\mu}=\boldsymbol{0}} \ \widehat{\mathbf{Q}}^{\mathrm{T}}\left[\mathbf{I}_{N_p}\mathbf{I}_{N_p}\right]\boldsymbol{\varepsilon} + \boldsymbol{\alpha}^{\mathrm{T}}\boldsymbol{\mu} \tag{25.a}$$

$$\text{s.t.} \ \ (21.\text{b}) \tag{25.b}$$

$$\mathbf{H}^{\mathrm{T}}\boldsymbol{\mu} - \mathbf{F}^{\mathrm{T}}\boldsymbol{\varepsilon} \ge 0 \tag{25.c}$$

$$\mathbf{I}^{\mathrm{T}}\boldsymbol{\mu} - \mathbf{G}^{\mathrm{T}}\boldsymbol{\varepsilon} \ge 0 \tag{25.d}$$

$$\left[\mathbf{I}_{N_p}\mathbf{I}_{N_p}\right]\boldsymbol{\varepsilon} \ge \boldsymbol{SPP}. \tag{25.e}$$

Since other constraints in (25) are linear, the whole problem boils down to the treatment of (25.e). Detach (25.e) into component-wise constraints and replace its right side with (11):

$$\left\{\left[\mathbf{I}_{N_p}\mathbf{I}_{N_p}\right]\boldsymbol{\varepsilon}\right\}_{(n)} \ge \max_{\boldsymbol{P}(z)\in\mathbb{W}(\boldsymbol{S}_n,\boldsymbol{h})} \int_{\Omega_z} SRP(\boldsymbol{u},z)\mathrm{d}\boldsymbol{P}(z), \forall n \tag{26}$$

Assign λ_n, $\boldsymbol{\tau}_n$, $\boldsymbol{\pi}_n^1$ and $\boldsymbol{\pi}_n^2$ as the dual variables for (21.a), (21.b) and (21.c), the integral operator can be eliminated by applying the strong duality theory.

$$\begin{aligned} \left\{\left[\mathbf{I}_{N_p}\mathbf{I}_{N_p}\right]\boldsymbol{\varepsilon}\right\}_{(n)} \ge & \min_{(\lambda_n,\boldsymbol{\tau}_n,\boldsymbol{\pi}_n^1,\boldsymbol{\pi}_n^2)\in\mathbb{W}_n^{\mathrm{D}}} \lambda_n + \left[\mathbf{1}^{N_l} - \boldsymbol{S}_{nl}\right]^T\boldsymbol{\tau}_n \\ & - \boldsymbol{P}_{n,\min}^{K\ \mathrm{T}}\boldsymbol{\pi}_n^1 + \boldsymbol{P}_{n,\max}^{K\ \mathrm{T}}\boldsymbol{\pi}_n^2, \forall n \end{aligned} \tag{27}$$

$$\mathbb{W}_n^{\mathrm{D}} = \left\{ \lambda_n, \boldsymbol{\tau}_n, \boldsymbol{\pi}_n^1, \boldsymbol{\pi}_n^2 \;\middle|\; \begin{array}{rl} \lambda_n + \boldsymbol{z}^{\mathrm{T}}\boldsymbol{\tau}_n - \boldsymbol{\delta}_{\boldsymbol{K}}(z)^{\mathrm{T}}\left(\boldsymbol{\pi}_n^1 - \boldsymbol{\pi}_n^2\right) - SRP(\boldsymbol{u},z) \ge \boldsymbol{0} & \\ \quad \forall \boldsymbol{z} \in \Omega_z & (28.\text{a}) \\ \boldsymbol{\pi}_{\mathrm{n}}^1, \boldsymbol{\pi}_{\mathrm{n}}^2 \ge 0 & (28.\text{b}) \end{array} \right\}$$

where

$$SRP(\boldsymbol{u},\boldsymbol{z}) = \min_{\boldsymbol{x}} \mathbf{c}^{\mathrm{T}}\boldsymbol{x} \tag{29.a}$$

$$\text{s.t.} \ \ \mathbf{J}\boldsymbol{x} + \mathbf{L}\boldsymbol{u} + \mathbf{M}\boldsymbol{z} \ge \boldsymbol{e} : [\boldsymbol{\xi}] \tag{29.b}$$

$\mathbf{1}^{N_l}$ is a $N_l \times 1$ vector with all elements set to 1. $\boldsymbol{\delta}_{\boldsymbol{K}}(z)$ is mapped to 1 when the number of element 1 in $\boldsymbol{z}$ is K. The coefficients of $\boldsymbol{\varepsilon}$ on the left side of (27) are always nonnegative and $(\boldsymbol{u},\boldsymbol{h},\boldsymbol{\lambda}_n,\boldsymbol{\tau}_n,\boldsymbol{\pi}_n^1,\boldsymbol{\pi}_n^2)$ are independent of $\boldsymbol{\varepsilon}$ and $\boldsymbol{\mu}$. This indicates that imposing smaller value on its right side will relax the constraint and lead to an objective value no worse than the original one. The right side of (27) will be automatically minimized under $\mathbb{W}_n^{\mathrm{D}}$ if (25.a) is to be optimized. Therefore, the min(·) in (24) could be removed with no impact on the result of (25).

Constraint (28) requires that (28.a) holds for all possible $\boldsymbol{z}$. The discrete nature of $\boldsymbol{z}$ denies the application of duality theory. At this point, an iterative dual cutting plain addition algorithm (Algorithm 3) can be employed to solve this problem.

B. Sparsification of Failure State Space

In the solution procedure of Section IV-A, the computational challenge primarily comes from the size of failure state space (FSS), Ω_z in SPP. Larger Ω_z requires more failure scenario $\widehat{z}^r$ to be identified in Algorithm 3 so that (28.a) can hold.

The problem becomes more serious for FSS with high contingency level (FSS-H), compared to that with low contingency

Algorithm 3 Dual Cutting Plain Addition Algorithm for DTDP

Step 1: Set the current bound CB $= -\infty$, the number of iteration r=1, the index of the current RP in the subproblem n=1. The collective set of cutting planes from the subproblems are denoted as CUT^r. $CUT^1 = \varnothing$.

Step 2: Solve the following master problem.

$$\mathbf{MP}^r = (22.\mathrm{a}) \tag{30.a}$$

$$\text{s.t.}(22.\mathrm{b}-22.\mathrm{d}, 25.\mathrm{b}),\ \mathrm{CUT}^r$$

$$\left\{\left[\boldsymbol{I}_{N_p}\boldsymbol{I}_{N_p}\right]\boldsymbol{\varepsilon}\right\}_{(n)} \geq \lambda_n + [\mathbf{1}^{N_l} - \boldsymbol{S}_{nl}]^{\mathrm{T}}\tau_n - \boldsymbol{P}^K_{n,\min}{}^{\mathrm{T}}\boldsymbol{\pi}^{\mathbf{1}}_n \tag{30.b}$$

$$+ \boldsymbol{P}^K_{n,\max}{}^{\mathrm{T}}\boldsymbol{\pi}^2_n, \forall n. \tag{30.c}$$

Obtain the solution $(\widehat{\boldsymbol{u}}^r, \widehat{\boldsymbol{h}}^r, \widehat{\boldsymbol{\lambda}}^r_n, \widehat{\boldsymbol{\tau}}^r_n, \widehat{\boldsymbol{\pi}}^{1,r}_n, \widehat{\boldsymbol{\pi}}^{2,r}_n)$ at the r^{th} iteration and update CB using $\mathbf{MP}^r$.

Step 3: By taking the dual of SRP in (34), establish the subproblem

$$\mathbf{SP}^r = \max_{\boldsymbol{\xi}\geq 0, z\in\Omega_z} \boldsymbol{e}^{\mathrm{T}}\boldsymbol{\xi} - \widehat{\lambda}^r_n - z^{\mathrm{T}}\widehat{\boldsymbol{\tau}}^r_n + \boldsymbol{\delta}_{\boldsymbol{K}}(\mathrm{z})^{\mathrm{T}}\left(\widehat{\pi}^{1,\mathrm{r}}_{\mathrm{n}} - \widehat{\pi}^{2,\mathrm{r}}_{\mathrm{n}}\right) \tag{31.a}$$

$$\mathbf{J}^{\mathrm{T}}\boldsymbol{\xi} \leq \boldsymbol{c} \tag{31.b}$$

$$\left(\mathbf{1}^{N_l}\right)^{\mathrm{T}} z = \langle K_{\max}\rangle^{\mathrm{T}}\boldsymbol{\delta}_K(z) \tag{31.c}$$

$$\left(\mathbf{1}^{N_l}\right)^{\mathrm{T}}\boldsymbol{\delta}_K(z) = 1 \tag{31.a}$$

$$\boldsymbol{\delta}_K(z) \in \{0,1\}^{K_{\max}} \tag{31.a}$$

where $\langle K_{\max}\rangle = [1, 2, \ldots, K_{\max}]^{\mathrm{T}}$. Solve (31.a) and obtain the corresponding $(\widehat{\boldsymbol{\xi}}^r, \widehat{z}^r, \widehat{\boldsymbol{\delta}}_K(z)^r)$. If $\mathbf{SP}^r \leq \sigma$ (σ is a small value), the search of $\boldsymbol{z}$ over the n^{th} RP is finished. Set $n = n+1$. If $n > N_p$, then STOP; else, REDO **Step 3**. If $\mathbf{SP}^r > \sigma$, GOTO Step 4.

Step 4: Based on the results of the subproblem, generate two kinds of cutting planes

1) Primal Cut:

$$\mathrm{NC}^{r,\mathrm{Primal}} = \left\{ \begin{array}{c} \boldsymbol{c}^{\mathrm{T}}\boldsymbol{x}^r - \lambda_n - \widehat{z}^{r\mathrm{T}}\widehat{\boldsymbol{\tau}}^r_n + \widehat{\boldsymbol{\delta}}_K(z)^{r\,\mathrm{T}}_n\left(\boldsymbol{\pi}^1_n - \boldsymbol{\pi}^2_n\right) = 0, \forall n \\ \mathbf{J}\boldsymbol{x}^r + \mathbf{L}\boldsymbol{u} + \mathbf{M}\widehat{\boldsymbol{z}}^r \geq \boldsymbol{e} \end{array} \right\} \tag{32}$$

2) Dual Cut:

$$\mathrm{NC}^{r,\mathrm{Dual}} = \{\boldsymbol{e}^{\mathrm{T}}\widehat{\boldsymbol{\xi}}^r_n - \lambda_n - \widehat{\boldsymbol{z}}^{r\,\mathrm{T}}_n\widehat{\boldsymbol{\tau}}^r_n + \widehat{\boldsymbol{\delta}}_K(z)^{r\,\mathrm{T}}_n\left(\boldsymbol{\pi}^1_n - \boldsymbol{\pi}^2_n\right) = 0, \forall n\} \tag{33}$$

Update $\mathrm{CUT}^{r+1} = \{\mathrm{CUT}^r, \mathrm{NC}^{r,\mathrm{Primal}}, \mathrm{NC}^{r,\mathrm{Dual}}\}$, $r = r+1$, GOTO **Step 2**.

level (FSS-L). For example, for a system with 30 transmission lines, more than 1.4×10^5 states exist in the fifth-level FSS.

A sparsification method is proposed to slash the number of states in the original FSS. The method is implemented on the subspace of FSS, Ω_{zK}, corresponding to each contingency level. Two basic principles are suggested to maintain the same characteristic of the sparsified space, Ω'_{zK} to the original one, Ω_{zK}:

- *Unbiasedness:* The times of each line participate in all states of Ω'_{zK} should remain the same so that Ω'_{zK} will not be biased towards certain lines. This property has already been guaranteed in the original space Ω_{zK}.
- *Representativeness:* The overall severity of Ω'_{zK}, judged by the consequence of each state, should be close to that of Ω_{zK}. This ensures that Ω'_{zK} can drive the DTDP model to yield more stable results compared to a randomly generated FSS with the same number of states.

Next, a generation technique of Ω'_{zK} is suggested while satisfying the above principles. A large enough non-repetitive sample matrix $\boldsymbol{SP}_K$ is first obtained from Ω_{zK} by Monte Carlo method:

$$\boldsymbol{SP}_K = \begin{bmatrix} \boldsymbol{SP}_{K1} \\ \boldsymbol{SP}_{K2} \\ \vdots \\ \boldsymbol{SP}_{Ks} \\ \vdots \\ \boldsymbol{SP}_{KN_s} \end{bmatrix} = \begin{bmatrix} z_{11} & z_{12}\cdots & z_{1l}\cdots & z_{1N_l} \\ z_{21} & z_{22}\cdots & z_{2l}\cdots & z_{2N_l} \\ \vdots & \vdots\ \ddots & \vdots\ \ddots & \vdots \\ z_{s1} & z_{s2}\cdots & z_{sl}\cdots & z_{sN_l} \\ \vdots & \vdots\ \ddots & \vdots\ \ddots & \vdots \\ z_{N_s1} & z_{N_s2}\cdots & z_{N_sl}\cdots & z_{N_sN_l} \end{bmatrix} \tag{34}$$

$$\sum_{l\in\Omega_l} z_l = K\forall s = 1, 2, \ldots N_s \tag{35}$$

where N_s represent the size of samples in $\boldsymbol{SP}_K$. Let SRP_s be the result of SRP under the s^{th} sampled state before defense planning, which indicates the severity of its consequence:

$$SRP_s = SRP(\boldsymbol{u} = \mathbf{0}, \boldsymbol{SP}_{Ks}) \tag{36}$$

We further allocate all SRP_s into N_m uniformly divided bins based on their values. The corresponding SRP results for bin m is gathered in a vector SRP_{Km} with mean value calculated as $\overline{SRP_{bm}}$. $\boldsymbol{SP}_K$ is divided accordingly into $\boldsymbol{SP}_{K1}, \ldots, \boldsymbol{SP}_{KN_m}$. Suppose the number of samples in each bin are $N_{b1}, \ldots, N_{bm}, \ldots, N_{bN_m}$ and Ω'_{zK} need to extract N'_{bm} samples from bin m. $N_{\mathrm{b}m}{}'$ can be set to:

$$N_{\mathrm{b}m}{}' = \mathrm{round}\left(\frac{N_{\mathrm{b}N_m}}{N_s}\cdot\left|\Omega'_{zK}\right|\right) \tag{37}$$

where $|\Omega'_{zK}|$ is the desired number of states in Ω'_{zK}. Then, an auxiliary problem is established to pick the reserved states in Ω'_{zK}:

$$\min\ \left\|\boldsymbol{dev}^{1+} + \boldsymbol{dev}^{2+}\right\| \tag{38.a}$$

$$\text{s.t.}\ \left[\boldsymbol{sel}^{\mathrm{T}}_{\mathrm{b}1}\boldsymbol{sel}^{\mathrm{T}}_{\mathrm{b}2}\cdots\boldsymbol{sel}^{\mathrm{T}}_{\mathrm{b}N_m}\right]\cdot\left[\boldsymbol{SP}^{\mathrm{T}}_{K1}\boldsymbol{SP}^{\mathrm{T}}_{K1}\cdots\boldsymbol{SP}^{\mathrm{T}}_{K\mathrm{N_m}}\right]^{\mathrm{T}}$$

$$+ \boldsymbol{dev}^{1+} - \boldsymbol{dev}^{1-} = K\cdot\frac{N_s}{N_l} \tag{38.b}$$

$$\boldsymbol{sel}^{\mathrm{T}}_{\mathrm{b}m}\boldsymbol{SRP}_{Km} + \boldsymbol{dev}^{2+}_m - \boldsymbol{dev}^{2-}_m = \overline{SRP_{\mathrm{b}m}}, \forall m \tag{38.c}$$

$$dev^{2+}_m + dev^{2-}_m \leq Tol_m\cdot\overline{SRP_{\mathrm{b}m}}, \forall m \tag{38.d}$$

$$\left\|\boldsymbol{sel}^{\mathrm{T}}_{\mathrm{b}m}\right\| = N_{bm}{}', \forall m \tag{38.e}$$

$$\boldsymbol{dev}^{1+}, \boldsymbol{dev}^{1-}, dev^{2+}_m, dev^{2-}_m \geq 0, \forall m \tag{38.f}$$

where $\boldsymbol{sel}_{\mathrm{b}m}$ represents the selection variable. If $\boldsymbol{sel}_{bms} = 1$, then sample s from $\boldsymbol{SP}_{Km}$ is selected into Ω'_{zK}. The discrepancy between ideal participation times of each line and its actual participation times in $\Omega'_{\mathrm{z}K}$ is measured by $\boldsymbol{dev}^{1+}$ and $\boldsymbol{dev}^{1-}$ in constraints (38.b). They are minimized in (38.a) to ensure the unbiasedness of Ω'_{zK}. dev^{2+}_m and dev^{2-}_m measure the difference between $\boldsymbol{sel}^{\mathrm{T}}_{\mathrm{b}m}\boldsymbol{SRP}_{Km}$ (the averaged SRP result of the selected samples in bin m) and $\overline{SRP_{bm}}$ in (38.c), which is bounded by a tolerance level Tol_m in (38.d). Together, (38.c) and (38.d) ensure the representativeness of Ω'_{zK} is respected.

Following the solution of (38), $\Omega'_{\mathrm{z}K}$ could be formed by extracting samples from $\mathrm{SP_K}$ based on $\mathrm{sel_{bm}}$. A simplified model that replace $\Omega_{\mathrm{z}K}$ by $\Omega'_{\mathrm{z}K}$ in (21) can be established. The

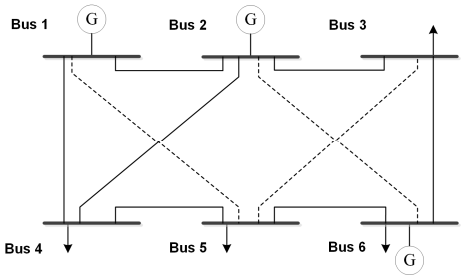

Fig. 3. Diagram of the modified six-bus test system.

TABLE I
PARAMETERS OF LOAD AND GENERATORS IN THE 6-BUS SYSTEM

No.	Real Load (MW)	Generator Bus	Capacity
1	0	√	100
2	0	√	150
3	31.2	×	-
4	102.4	×	-
5	83.5	×	-
6	38.9	√	100

TABLE II
PARAMETERS OF EXISTING AND CANDIDATE LINES IN THE 6-BUS SYSTEM

No.	From	To	R (p.u.)	X (p.u.)	Existing/candidate	Capacity (MW)	Cost ($/km·MW)
1	1	2	0.005	0.170	Existing	100	-
2	2	3	0	0.037	Existing	100	-
3	1	4	0.003	0.258	Existing	100	-
4	2	4	0.007	0.197	Existing	200	-
5	4	5	0	0.037	Existing	100	-
6	5	6	0.002	0.140	Existing	100	-
7	3	6	0	0.018	Existing	100	-
8	1	5	0.005	0.170	Candidate	100	1000
9	2	6	0	0.037	Candidate	100	1000
10	3	5	0	0.037	Candidate	100	1000

effect of the FSS sparsification method is further discussed in Section V-B.

V. CASE STUDIES

Case studies have been conducted on a modified 6-bus test system [36] and the RTS-79 system to demonstrate the advantages of the proposed DTDP model. Candidate transmission lines are selected by the automatic candidate discovery method developed in [37]. All cases were carried out on Intel Core i5-6500 with Gurobi 8.1.0 on MATLAB 2017b.

A. Modified 6-Bus Test System

The diagram and detailed information of the modified 6-bus system is given in Fig. 3, Table I and Table II. The buses in the system are mapped to the Qingyuan-Meizhou region of Guangdong Province, China with basic profile of windstorm events provided by the Tropical Data Center of China Meteorological Administration [38]. The cyclone simulation model in [39] was also used to supplement the data set.

(1) *Comparison to the modified DAD model:* A modified DAD model using information theory-based uncertainty set [24] (denoted as M-DAD) is also implemented in this section. M-DAD can account for component survivability and is suitable for comparison. Since the DAD models do not distinguish between different extreme events, the number of RP in SPP is set to 1. In this case, DTDP is regarded as a short-term hardenning problem targeting the imminent event, and the line construction is prohibited. The budget in (13.c) is set to 400 m$.

TABLE III
TRANSMISSION LINE SURVIVABILITY UNDER A WEATHER EVENT

No	Survivability (%)			Hardening Cost ($/km·MW)	
	A	B	C	B	C
1	81.9	85.7	86.9	400	1000
2	86.4	90.2	92.2	400	1000
3	83.3	86.4	87.4	400	1000
4	83.1	88.7	90.2	400	1000
5	84.2	89.5	90.8	400	1000
6	92.2	95.5	96.6	400	1000
7	90.3	92.9	94.5	400	1000
8	85.2	89.2	91.2	400	1000
9	86.2	89.8	91.6	400	1000
10	89.2	92.4	94.6	400	1000

TABLE IV
COMPARISON BETWEEN THE PROPOSED DTDP MODEL AND M-DAD MODEL

Model Type		Before Planning	Proposed Model	M-DAD Model		
				UB=5.0	UB=10.0	UB=15.0
Hardening plan for transmission lines	1	A*	A	A	A	A
	2	A	C	A	C	A
	3	A	A	A	C	A
	4	A	C	A	C	B
	5	A	C	A	A	A
	6	A	C	A	A	B
	7	A	A	A	C	A
WCEL (MW)		**25.89**	**17.80**	**25.89**	**21.57**	**22.34**
EPNS-E (MW)		**7.72**	**3.51**	**7.72**	**4.19**	**5.49**

The cost of various hardening plans and the calculated results of component survivability are given in Table III. Without loss of generality, the effects of three hardening plans (denoted as A, B, C) are distinguished by multiplying 0.9, 0.7 and 0.6 to κ in (1), whose base value is given in [40]. The hardening plans are for the transmission line segments as well as the towers. Plan A denotes the case without hardening implemention and Plan C denotes the most effective hardening plan.

Two indices are used to evaluate the performance before the defense planning and that after the defense planning. They are WCEL (worst-case expected loadshed) in (8) and EPNS-E in (5). EPNS-E serves as a benchmark and is independently calculated by the Monte-Carlo simulation after the defense plan is obtained. The M-DAD model considers three uncertainty budgets (UB): UB = 5, 10, and 15.

Simulation results are shown in Table IV. Note that M-DAD fails to use up the budget when UB is 5.0 and 15.0. When the UB is set too low, no failure state will be identified to justify the adoption of hardening plan. When it is set too

TABLE V
SYSTEM LOSS INDICES COMPARISON BETWEEN THE PROPOSED DTDP MODEL AND STOCHASTIC OPTIMIZATION MODEL

Proposed				Stochastic Optimization					
N_p	WCEL (MW)	EPNS-E (MW)	CPU Time (s)	N_p	N_s	Obj. (MW)	EPNS-E (MW)	WCEL (MW)	CPU Time (s)
2	11.26	0.954	85.2	4	50	0.00	1.372	15.61	0.8
					100	0.13	1.389	13.96	65.1
4	10.04	0.802	129.3		200	0.42	1.316	14.71	322.5
					400	0.43	1.177	13.34	806.7
8	10.33	0.748	191.4	8	50	0.21	1.602	16.08	73.3
					100	0.64	1.489	15.21	385.0
12	10.47	0.750	300.3		200	0.85	1.188	13.18	1386.1
					400	0.75	1.134	12.40	3030.2
16	10.65	0.750	316.0	12	50	0.25	1.188	13.75	133.7
					100	0.55	1.198	13.83	607.3
20	10.67	0.751	354.0		200	0.58	1.099	12.91	1634.6
					400	0.78	0.935	12.07	9054.1

*obj.: the value of objective function for SO when it is solved.

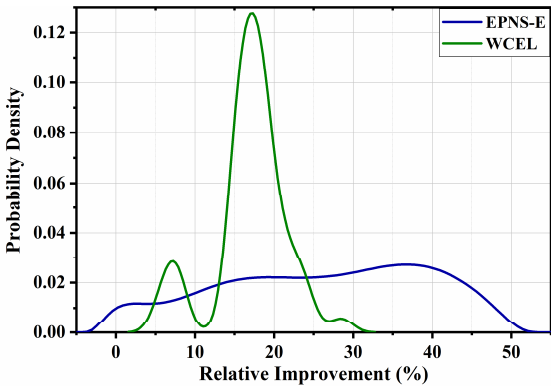

Fig. 4. Relative improvement compared to M-DAD Model (UB=10.0).

high, no hardening plan will be enough to raise the component survivability above the UB. Therefore, the model is forced to terminate. On the other hand, the proposed model is free from the influence of UB. Therefore, an optimal defense plan making full use of the budget can always be obtained. This characteristic is particularly valuable due to the fact that the survivability of transmission network during a windstorm is usually higher than the overhead lines in a distribution network [41], making it more difficult for the decision maker to find an appropriate UB.

Even when the budget is completely used in both models, the DTDP is able to find a better plan than M-DAD (UB=10.0), as it results in lower WCEL and EPNS-E. To further illustrate the performances, both models are applied to 50 different extreme events. The relative improvement of DTDP compared to M-DAD is calculated and represented as a PDF plot in Fig. 4. The majority of the plot lies on the positive axis, indicating the superiority of DTDP in resource allocation. Actually, the average improvement on EPNS-E and WCEL are 26.1% and 17.0% respectively.

(2) *Comparison to the stochastic optimization model.* In this section, performance of the proposed DTDP model is compared with that of the stochastic optimization (SO) model in terms of the loss indices WCEL and EPNS-E. For SO, the technique in [12] is used to reduce the number of scenarios and the method in [14] is applied to capture the decision-dependent uncertainty caused by line hardening.

Table V shows the results of WCEL, EPNS-E, and computation time by the proposed DTDP and SO methods. For DTDP model, 100 events are included in the target event set. Different numbers of RPs, N_p, were considered. For stochastic optimization, N_s failure scenarios are included for each representative extreme event. Thus, there are $N_s \times N_p$ scenarios in total. It is observed from Table V that the DTDP model can deliver satisfactory results even with a few RPs. The results converge quickly as the number of RPs increases. Another important finding from Table V is that DTDP can obtain plans that perform better in terms of both WCEL and EPNS-E, although DTDP is designed to minimize WCEL, which is essentially a robust upper bound on EPNS-E. On the other hand, SO fails to obtain a stable approximation of EPNS-E (by comparing the column of obj. and EPNS-E) and its computation time grows rapidly when the number of scenarios increases.

(3) *Effectiveness of line construction and hardening.* To investigate the respective contribution of line construction and hardening under different budget, three options are considered.

S1: Line construction and line hardening are permitted.

S2: Only line construction is permitted.

S3: Only line hardening of the existing line is permitted.

The effects of defense strategies on WCEL are evaluated under various budget constraints ranging from 0 to 1,500 m$. Fig. 5 illustrates the system loss under various defense options and budget. It is observed from Fig. 5 that the loss index WCEL are gradually declined as the budget is increased. In S2, the construction of different lines could have disparate effectiveness. For example, WCEL in S2 drops dramatically when line 8 is built under the 100 m$ budget since it connects the generation bus 1 and the load bus 5. This effect is less pronounced when more lines are built. On the other hand,

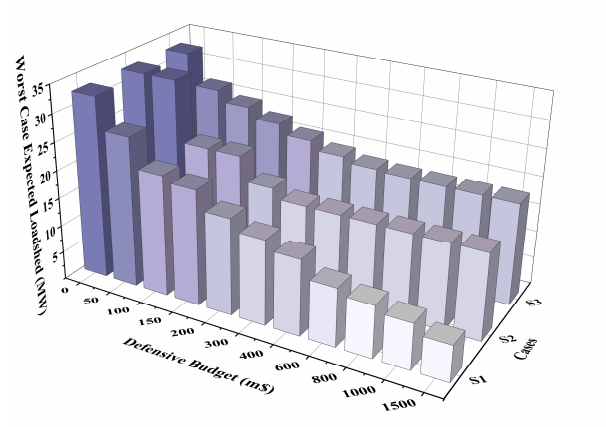

Fig. 5. System loss under different defense options and budget.

TABLE VI
DEFENSE MEASURE UNDER DIFFERENT DEFENSE BUDGET IN SCENARIO 1

Budget (m$)	Number of Line										WCEL (MW)
	1	2	3	4	5	6	7	8	9	10	
0	A	A	A	A	A	A	A	-	-	-	**32.73**
50	A	A	A	B	A	A	A	-	-	-	**26.98**
100	A	A	A	A	A	A	A	A	-	-	**21.68**
150	A	A	A	B	A	A	A	A	-	-	**20.69**
200	A	A	A	A	A	A	A	A	-	A	**17.33**
300	A	B	A	A	A	A	A	B	-	A	**15.32**
400	A	A	A	A	A	B	B	A	A	A	**13.60**
600	A	C	A	C	A	C	A	C	A	A	**10.47**
800	B	C	B	B	B	C	C	C	A	B	**9.39**
1000	B	C	B	B	B	C	C	C	B	C	**8.29**
1500	C	C	C	C	C	C	C	C	C	C	**6.53**

the hardening strategy (S3) lowers the WCEL in a smooth but slow manner. Consideration of both the line construction and the line hardening strategies yields better results than just a single strategy.

Table VI details the defense plan and the corresponding WCEL in S1 to further elucidate the effect of budget constraint. Raising the budget is effective in reducing the WCEL when system resilience is relatively low. For example, WCEL could be reduced from 32.73 MW to 26.98 MW by merely hardening line 4. Besides, when the budget is raised from 600 m$ to 800 m$, the hardening plan for line 4 changes from Plan C to Plan B. This allows lines 1, 5, and 10 to be hardened. This change indicates that the number of hardened lines is more important than the hardening level under this circumstance.

(4) *Effect of target event selection:* Section II has discussed the effect of target event selection on the DTDP model. Here, the severity of target events is used to verify such effect. The severity of target events can be divided into five classes based on their EPNS-E before planning. Class 1 denotes the events with EPNS-E in the range of [0, 4) MW, and Class 5 denotes that higher than 12 MW. The effectiveness of the defense plan is further checked under three budget levels: low investment (300 m$), medium investment (600 m$), and high investment (1000 m$).

TABLE VII
EFFECT OF DTDP AGAINST TARGET EVENTS OF DIFFERENT CLASSES

Class of Target Events	Range of EPNS-E (MW)	Worst Case Expected Loadshed (MW)			
		No investment	Low investment	Medium investment	High investment
1	[0, 4)	23.26	8.78 (-62.3%)	7.47 (-67.9%)	5.35 (-77.0%)
2	[4, 8)	29.86	13.34 (-55.3%)	11.17 (-62.6%)	7.65 (-74.4%)
3	[8, 10)	35.52	17.59 (-50.5%)	14.78 (-58.4%)	10.71 (-69.8%)
4	[10, 12)	40.83	22.42 (-45.1%)	18.78 (-54.0%)	14.17 (-65.3%)
5	[12, +∞)	46.08	27.74 (-39.8%)	22.94 (-50.2%)	17.86 (-61.2%)

TABLE VIII
SUMMARY OF RTS-79 NUMERICAL EXAMPLE

Buses	24	Generators	32
Existing lines	35	Line hardening cost ($/km·MW)	400
Candidate Lines	10	Line construction cost ($/km·MW)	1000
Number of TE	100	Range of *WCSDR* for TE (%)	[0, 5]
Number of RP	5	Defensive Budget (m$)	1000

Table VII shows the WECLs of various classes with different budgets. It is observed from Table VII that the target events with higher severity produce larger WCEL outputs of the DTDP model. This shows that higher budget is required to reduce WCEL to a desired value. For example, low investment is sufficient to keep the WCEL of class-3 events under 20 MW, whereas high investment is needed to achieve the same objective for class-5 events.

Moreover, the defense planning tends to have smaller impact on the extreme events of higher classes under the same amount of budgets. The defense plan with low investment deteriorates faster than that with high investment. For example, the WCEL of class-5 events with low investment is reduced by 39.8% from that with no investment, while that with high investment is reduced by 61.2%. Thus, with the increased severity of extreme events, the decision maker may consider to raise the investment to maintain the same level of performance improvement.

(5) *Influence from the number of target events:* The impact of the number of target events (level-3) on system loss is illustrated in Fig. 6, which displays the WCELs with and without the Wasserstein metric. It can be seen from Fig. 6 that, in both cases, WCEL decreases as the number of target events grows. This means that the DTDP model possesses a better understanding about the pattern of extreme events when more information is available. Thus, less conservative estimates of WCEL could be obtained.

The convergence curve with Wasserstein metric performs better than that without Wasserstein metric because the former obtains smaller WCEL even when only a few events serves as inputs. This property is particularly useful considering that

TABLE IX
OPTIMAL DEFENSE PLANS OF RTS-79 NUMERICAL EXAMPLE

Case	Number of states in sparsified FSS	Hardened Transmission Line	Constructed Candidate Line	$\widetilde{W}$ (MW)	$\widehat{W}$ (MW)	$\overline{E}$ (MW)
0	Original	/	/	/	260.28	98.27
1	2×10^3	2-6, 3-24, 6-10, 9-11, 9-12, 10-11, 10-12, 11-13, 12-13, 14-16, 15-21, 15-24, 16-19, 7-8	1-5, 4-8, 7-8, 14-15	70.78	133.56 (-48.7%)	13.14 (-86.6%)
2	4×10^3	2-6, 3-24, 6-10, 9-11, 9-12,10-12, 11-13, 12-23, 15-21, 15-24, 16-17, 16-19, 7-8, 14-15	1-5, 4-8, 7-8, 14-15	75.03	118.37 (-54.5%)	13.97 (-85.8%)
3	8×10^3	2-6, 3-24, 6-10, 9-11, 10-11,10-12, 11-13, 12-23, 15-21, 15-24, 16-19, 20-23, 7-8,14-15	1-5, 14-24, 7-8, 14-15	78.91	115.30 (-55.7%)	11.98 (-87.8%)
4	1.6×10^4	2-6, 3-24, 6-10, 8-10, 9-11, 10-11, 10-12, 11-13, 15-21, 15-24, 19-20, 20-23, 7-8, 14-15	1-5, 6-9, 7-8, 14-15	80.20	114.55 (-55.9%)	11.97 (-87.8%)
5	Original	2-6, 3-24, 6-10, 9-11, 9-12, 10-12, 11-13, 12-23, 15-21, 15-24, 19-20, 20-23, 6-9, 7-8, 14-15	1-5, 6-9, 7-8, 14-15	108.80	108.80 (-58.2%)	10.72 (-89.1%)

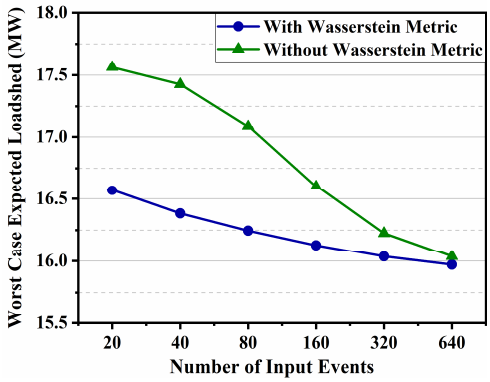

Fig. 6. Impact of the number of identified target events on WCEL.

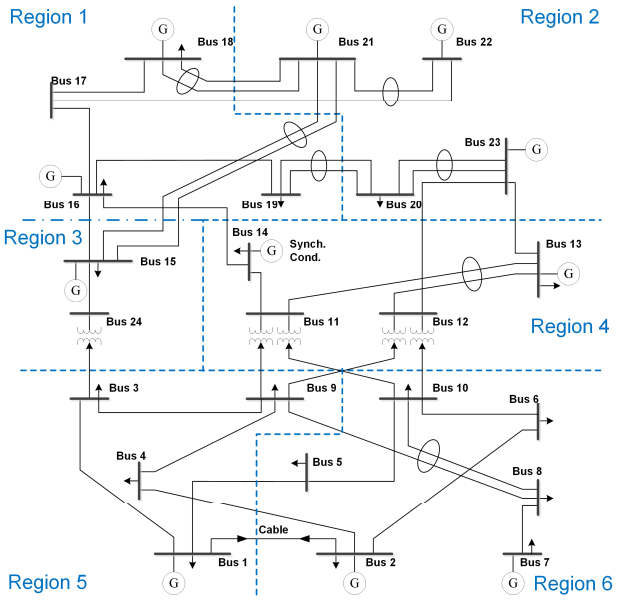

Fig. 7. Weather regions of the RTS-79 system.

the information about extreme events is limited compared to weather profile under normal condition.

B. Modified RTS-79 System

A modified RTS-79 system is used to demonstrate the performance improvement of the FSS sparsification method on the DTDP model. The whole system is divided into 6 regions as in Fig. 7. For an individual extreme event, the lines in the same region are assumed to undergo the same weather pattern. The approximate metric WCSDR is used to filter the target events. The transmission capacity of all lines is modified to 0.6 p.u. The maximum level of failure state is set to 7. Detailed information is summarized in Table VIII.

For low contingency level failure states, the original FSS is used. For those with high contingency level ($\geq$4), their FSS is sparsified using the method in Section IV-B. The total number of states in the sparsified FSS is set to 2×10^3, 4×10^3, 8×10^3, and 1.6×10^4 for Cases 1 to 4, respectively. Two additional cases are added. Case 0 implements no defense measure. Case 5 is similar to Cases 1 to 4 except that the sparsification method is not used.

The optimal defense plans are shown in Table IX. They are described as in the columns of hardened transmission line and the constructed candidate line. Columns of $\widetilde{W}$ and $\widehat{W}$ denote the results of the DTDP objective function (8). $\widetilde{W}$ is directly calculated from each case and $\widehat{W}$ is obtained by applying the defense plan of each case to the setting of Case 5. The average EPNS-E ($\overline{E}$) is obtained by averaging out system performance after planning under 25 extreme events out of Ω^{TE}. Both $\widehat{W}$ and $\overline{E}$ indicate the quality of solution.

It can be seen from Table IX that, in all cases, 15 lines are hardened and 4 new lines are constructed. The cases with fewer failure states return smaller $\widetilde{W}$, indicating that the loss of load is underestimated compared to the Case 5. This may slightly lower the quality of the solution because their $\widehat{W}$ and $\overline{E}$ are higher than case 5. Nonetheless, all cases are able to reduce $\widehat{W}$ by more than 50 % and $\overline{E}$ by 85 %. The only exception is case 1, which means that deterioration in the solution quality is acceptable. Increasing the number of states in FSS also delivers better solutions.

The test was repeated 30 times to evaluate the robustness and efficiency of the proposed sparsification method. Table X shows the 90% confidence interval of $\widetilde{W}$. It can be seen from Table X that lengths of the confidence intervals for all cases

TABLE X
ROBUSTNESS AND EFFICIENCY TEST OF RTS-79 NUMERICAL EXAMPLE

Case	90% Confidence Interval of $\widetilde{W}$ (MW)	Average CPU Time (hours)	Average Iterations
1	[69.70, 73.59]	0.92	90.5
2	[73.46, 76.44]	1.38	94.6
3	[77.59,80.09]	2.24	105.1
4	[79.21,82.20]	3.66	128.2
5	/	10.60	258.1

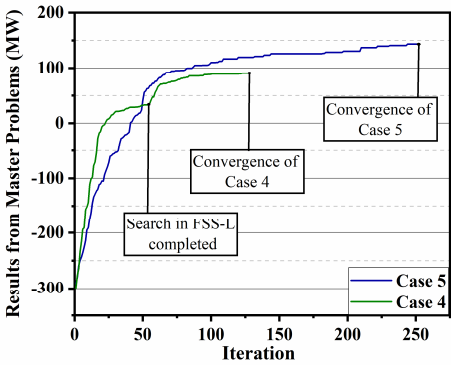

Fig. 8. The current bound returned from the master problem versus the iteration steps.

are within 6 % of their median. This implies that the method can yield stable outputs with the same number of failure states. The average CPU time and the number of iterations are also listed. The simplified model using the sparsification technique saves up to 91.32% computing time. It is more efficient when fewer states are reserved in the FSS. In conclusion, a tradeoff between efficiency and quality can be achieved by tuning the number of states for the sparsification method.

The evolution of current bound for Case 4 and Case 5 in Section V-B is illustrated in Fig. 8. Both cases are able to converge within finite iterations. Case 4 stops at a lower point compared to Case 5. This is due to the fact that only a portion of failure states is considered by the FSS sparsification method. The number of iteration as well as the average computation time consumed for each iteration in Case 4 are less than that in Case 5. The reasons for this efficiency improvement are:

1) FSS in Case 4 is curtailed. Thus, fewer failure states need to be included in the master problem of Algorithm 3 to ensure that (28.a) holds.

2) The curtailed FSS also contributes to the searching efficiency of subproblems due to the reduction of its feasible region.

VI. CONCLUSION

In this paper, a four-level distributionally robust optimization-based model has been presented for the data-driven defense planning of transmission network against extreme events. The probabilistic information derived from extreme events are selected by the proposed criterion and included in the model. Furthermore, efficiency of the model is greatly improved using the FSS sparsification method. Case studies on a 6-bus system and modified RTS-79 system demonstrate that the proposed model is able to describe extreme events by past information instead of human-made uncertainty budget; consider the impact of line hardening and line construction simultaneously; minimize the average economic loss under the worst-case probability distribution, and reduce the conservatism.

Findings of this study include the following: 1) Consideration of the failure state probability in the DTDP model yields a better defense plan regarding the system loss indices in comparison to that of the DAD models. 2) The proposed DTDP model outperforms the stochastic optimization method in terms of EPNS-E by minimizing the worst-case expected loadshed (WCEL). 3) Larger investment in defense planning is more likely to maintain consistent performance improvement against the extreme events of different levels. 4) Large historical data on extreme events enable the reduction of the estimated value of WCEL for the DTDP model and thus its conservatism.

Future work will focus on the extension of the proposed DTDP model 1) to consider the sequential line failures during extreme events, and 2) to coordinate with the transmission system restoration after the events. Possible tasks to be performed include the addition of more checkpoints along the timeline of extreme events and the incorporation of transmission line repair into the optimal system response.

REFERENCES

[1] Z. Bie, Y. Lin, G. Li, and F. Li, "Battling the extreme: A study on the power system resilience," *Proc. IEEE*, vol. 105, no. 7, pp. 1253–1266, Jul. 2017.

[2] E. Blake *et al.*, "Tropical cyclone report hurricane sandy 22–29 October 2012," Nat. Hurricane Center, Miami, FL, USA, Rep. AL182012, Feb. 2013.

[3] G. Brown, M. Carlyle, J. Salmerón, and K. Wood, "Defending critical infrastructure," *Interfaces*, vol. 36, no. 6, pp. 530–544, Nov./Dec. 2006.

[4] A. Stankovic, *The Definition and Quantification of Resilience*, IEEE PES Ind. Tech. Support Task Force, Piscataway, NJ, USA, Apr. 2018.

[5] M. Panteli and P. Mancarella, "Influence of extreme weather and climate change on the resilience of power systems: Impacts and possible mitigation strategies," *Elect. Power Syst. Res.*, vol. 127, pp. 259–270, Oct. 2015.

[6] R. A. Bakkiyaraj and N. Kumarappan, "Optimal reliability planning for a composite electric power system based on Monte Carlo simulation using particle swarm optimization," *Int. J. Elect. Power Energy Syst.*, vol. 47, pp. 109–116, May 2013.

[7] M. Panteli and P. Mancarella, "Modeling and evaluating the resilience of critical electrical power infrastructure to extreme weather events," *IEEE Syst. J.*, vol. 11, no. 3, pp. 1733–1742, Sep. 2017.

[8] R. Rocchetta, E. Zio, and E. Patelli, "A power-flow emulator approach for resilience assessment of repairable power grids subject to weather-induced failures and data deficiency," *Appl. Energy*, vol. 210, pp. 339–350, Jan. 2018.

[9] Y. H. Yang, W. H. Tang, Y. Liu, Y. Xin, and Q. Wu, "Quantitative resilience assessment for power transmission systems under typhoon weather," *IEEE Access*, vol. 6, pp. 40747–40756, 2018.

[10] A. I. Sarwat, M. Amini, A. Domijan, A. Damnjanovic, and F. Kaleem, "Weather-based interruption prediction in the smart grid utilizing chronological data," *J. Mod. Power Syst. Clean Energy*, vol. 4, no. 2, pp. 308–315, Apr. 2016.

[11] A. I. Sarwat, A. Domijan, M. H. Amini, A. Damnjanovic, and A. Moghadasi, "Smart grid reliability assessment utilizing boolean driven Markov process and variable weather conditions," in *Proc. North Amer. Power Symp.*, 2015, pp. 1–6.

[12] H. Heitsch and W. Römisch, "Scenario reduction algorithms in stochastic programming," *Comput. Optim. Appl.*, vol. 24, nos. 2–3, pp. 187–206, Feb./Mar. 2003.

[13] N. R. Romero, L. K. Nozick, I. D. Dobson, N. Xu, and D. A. Jones, "Transmission and generation expansion to mitigate seismic risk," *IEEE Trans. Power Syst.*, vol. 28, no. 4, pp. 3692–3701, Nov. 2013.
[14] S. S. Ma, L. Su, Z. Wang, F. Qiu, and G. Guo, "Resilience enhancement of distribution grids against extreme weather events," *IEEE Trans. Power Syst.*, vol. 33, no. 5, pp. 4842–4853, Sep. 2018.
[15] S. S. Ma, S. Y. Li, Z. Y. Wang, and F. Qiu, "Resilience-oriented design of distribution systems," *IEEE Trans. Power Syst.*, vol. 34, no. 4, pp. 2880–2891, Jul. 2019.
[16] B. Zhang, P. Dehghanian, and M. Kezunovic, "Optimal allocation of PV generation and battery storage for enhanced resilience," *IEEE Trans. Smart Grid*, vol. 10, no. 1, pp. 535–545, Jan. 2019.
[17] W. Yuan, L. Zhao, and B. Zeng, "Optimal power grid protection through a defender–attacker–defender model," *Rel. Eng. Syst. Safety*, vol. 121, pp. 83–89, Jan. 2014.
[18] Y. P. Fang and G. Sansavini, "Optimizing power system investments and resilience against attacks," *Rel. Eng. Syst. Safety*, vol. 159, pp. 161–173, Mar. 2017.
[19] N. Romero, N. X. Xu, L. K. Nozick, I. Dobson, and D. Jones, "Investment planning for electric power systems under terrorist threat," *IEEE Trans. Power Syst.*, vol. 27, no. 1, pp. 108–116, Feb. 2012.
[20] D. Bertsimas, D. B. Brown, and C. Caramanis, "Theory and applications of robust optimization," *SIAM Rev.*, vol. 53, no. 3, pp. 464–501, 2011.
[21] W. Yuan, J. H. Wang, F. Qiu, C. Kang, and B. Zeng, "Robust optimization-based resilient distribution network planning against natural disasters," *IEEE Trans. Smart Grid*, vol. 7, no. 6, pp. 2817–2826, Nov. 2016.
[22] C. C. Shao, M. Shahidehpour, X. Wang, X. Wang, and B. Wang, "Integrated planning of electricity and natural gas transportation systems for enhancing the power grid resilience," *IEEE Trans. Power Syst.*, vol. 32, no. 6, pp. 4418–4429, Nov. 2017.
[23] A. Bagheri, C. Y. Zhao, F. Qiu, and J. H. Wang, "Resilient transmission hardening planning in a high renewable penetration era," *IEEE Trans. Power Syst.*, vol. 34, no. 2, pp. 873–882, Mar. 2019.
[24] S. S. Ma, B. K. Chen, and Z. Y. Wang, "Resilience enhancement strategy for distribution systems under extreme weather events," *IEEE Trans. Smart Grid*, vol. 9, no. 2, pp. 1442–1451, Mar. 2018.
[25] C. He, C. X. Dai, L. Wu, and T. Q. Liu, "Robust network hardening strategy for enhancing resilience of integrated electricity and natural gas distribution systems against natural disasters," *IEEE Trans. Power Syst.*, vol. 33, no. 5, pp. 5787–5798, Sep. 2018.
[26] R. Jiang and Y. Guan, "Risk-averse two-stage stochastic program with distributional ambiguity," *Ope. Res.*, vol. 66, no. 5, pp. 1390–1405, 2018.
[27] R. Gao and A. J. Kleywegt, "Distributionally robust stochastic optimization with dependence structure," *arXiv preprint arXiv:1701.04200*, Jan. 2017.
[28] C. Wang, Y. H. Hou, F. Qiu, S. Lei, and K. Liu, "Resilience enhancement with sequentially proactive operation strategies," *IEEE Trans. Power Syst.*, vol. 32, no. 4, pp. 2847–2857, Jul. 2017.
[29] Y. F. Wang, L. Huang, M. Shahidehpour, L. L. Lai, H. Yuan, and F. Y. Xu, "Resilience-constrained hourly unit commitment in electricity grids," *IEEE Trans. Power Syst.*, vol. 33, no. 5, pp. 5604–5614, Sep. 2018.
[30] C. Duan, W. L. Fang, L. Jiang, L. Yao, and J. Liu, "Distributionally robust chance-constrained approximate AC-OPF with Wasserstein metric," *IEEE Trans. Power Syst.*, vol. 33, no. 5, pp. 4924–4936, Sep. 2018.
[31] C. Zhao and Y. Guan. *Data-Driven Risk-Averse Two-Stage Stochastic Program With ζ-Structure Probability Metrics[J]*. Accessed: Apr. 2015. [Online]. Available: http://www.optimization-online.org/DB_FILE/2015/07/5014.pdf
[32] X. Wang, G. Ruipeng, and Y. Cao, "A self-adapting stratified and importance sampling method for power system reliability evaluation," *Autom. Elect. Power Syst.*, vol. 35, pp. 33–38, Mar. 2011.
[33] A. Arab, A. Khodaei, Z. Han, and S. K. Khator, "Proactive recovery of electric power assets for resiliency enhancement," *IEEE Access*, vol. 3, pp. 99–109, 2015.
[34] Y.-P. Fang and G. Sansavini, "Optimum post-disruption restoration under uncertainty for enhancing critical infrastructure resilience," *Rel. Eng. Syst. Safety*, vol. 185, pp. 1–11, May 2019.
[35] C. Coffrin and P. Van Hentenryck, "A linear-programming approximation of AC power flows," *INFORMS J. Comput.*, vol. 26, no. 4, pp. 718–734, Nov. 2014.
[36] *Modified 6-Bus Test System Data*. Accessed: May 2019. [Online]. Available: http://motor.ece.iit.edu/data/PCUC_6bus.doc
[37] S. Lumbreras, A. Ramos, and P. Sánchez, "Automatic selection of candidate investments for transmission expansion planning," *Int. J. Elect. Power Energy Syst.*, vol. 59, pp. 130–140, Jul. 2014.
[38] *Tropical Data Center of China Meteorological Administration*. Accessed: Mar. 2019. [Online]. Available: http://tcdata.typhoon.org.cn/en/index.html
[39] Y. Meng, M. Matsui, and K. Hibi, "An analytical model for simulation of the wind field in a typhoon boundary layer," *J. Wind Eng. Ind. Aerodyn.*, vol. 56, nos. 2–3, pp. 291–310, May 1995.
[40] G. Li *et al.*, "Risk analysis for distribution systems in the Northeast U.S. under wind storms," *IEEE Trans. Power Syst.*, vol. 29, no. 2, pp. 889–898, Mar. 2014.
[41] Executive Office of the President. (2013). *Economic Benefits of Increasing Electric Grid Resilience to Weather Outages—August 2013*. [Online]. Available: https://www.energy.gov/sites/prod/files/2013/08/f2/GridResiliencyReport_FINAL.pdf

Jiahao Yan (S'17) received the B.E. degree from the Hefei University of Technology, China, in 2016. He is currently pursuing the Ph.D. degree with Chongqing University, China. His research interests include power system risk assessment and optimization.

Bo Hu (M'14) was born in Henan, China, in 1983. He received the Ph.D. degree in electrical engineering from Chongqing University, Chongqing, China, in 2010, where he is a Professor with the School of Electrical Engineering. His research interests include power system reliability and parallel computing techniques in power systems.

Kaigui Xie (M'10–SM'13) is a Full Professor with the School of Electrical Engineering, Chongqing University, China. His main research interests focus on areas of power system reliability, planning, and analysis. He is an Editor of the IEEE TRANSACTIONS ON POWER SYSTEMS.

Junjie Tang (M'14) received the Ph.D. degree in electrical engineering from the E.ON Energy Research Center, Institute for Automation of Complex Power Systems, RWTH Aachen University, Aachen, Germany, in 2014. He is currently an Associate Professor with the State Key Laboratory of Power Transmission Equipment and System Security and New Technology, Power and Energy Reliability Research Center, School of Electrical Engineering, Chongqing University, Chongqing, China. His current research interests include power system uncertainty quantification analysis, power system security risk assessment and optimal management, and modeling of hybrid ac/dc grid.

Heng-Ming Tai (M'87–SM'94) is a Professor with the Department of Electrical and Computer Engineering, University of Tulsa, OK, USA. His research interests include power system reliability and industrial electronics.